SCIENTIFIC ARTICLE

Distal Radius Volar Locking Plate Design and Associated Vulnerability of the Flexor Pollicis Longus

Roongsak Limthongthang, MD, Abdo Bachoura, MD, Sidney M. Jacoby, MD, A. Lee Osterman, MD

Purpose Flexor pollicis longus (FPL) tendon rupture is a well-documented complication related to the use of distal radius volar locking plates (VLPs). The final common pathway of flexor tendon rupture appears to involve implants prominent at the watershed line. We hypothesized that significant differences in VLP prominence exist between various plate designs.

Methods Ten fresh frozen specimens were dissected to identify the path of the FPL in relationship to the distal radius at the watershed line. Five VLP designs were fixed to each specimen based on their anatomic fit, and slid distally until the distal edge of the plate reached the watershed line. The position of each fixed plate was evaluated by fluoroscopy. We used a 3-dimensional laser scanner to create computer models. The total surface area of plate prominence volar to the watershed line and the prominent area beneath the FPL were measured in the axial plane using computer software.

Results At the watershed line, the FPL was located at 54% of the maximal width of the radius, as measured from its volar-ulnar corner. There were no significant differences in the location of plate fixation on lateral view radiographs according to the classification of Soong et al. The mean total surface area of plate prominence was 36 mm^2. The mean prominent area beneath the FPL was 10 mm^2. Significant differences in plate prominence were noted for various designs.

Conclusions Despite optimal plate placement, various VLP designs were observed to have prominent profiles volar to the watershed line, to varying extents.

Clinical relevance The results raise concerns regarding interference between all of the analyzed VLP designs and the FPL. This study may help guide both implant design considerations and assist the surgeon in better understanding implant morphology as it relates to iatrogenic flexor tendon injury. *(J Hand Surg Am. 2014;■:■−■. Copyright © 2014 by the American Society for Surgery of the Hand. All rights reserved.)*

Key words Distal radius fracture, flexor tendon rupture, plate prominence, volar plating, watershed line.

The treatment of distal radius fractures has evolved considerably over the past decade owing to advancements in implant technology and surgical techniques. Since its introduction in 2000,[1] the volar locking distal radius plate (VLP) has become the workhorse for the treatment of unstable distal radius fractures. The frequency of the use of these plates has more than doubled over the past

From the Philadelphia Hand Center, Department of Orthopaedic Surgery, Thomas Jefferson University, Philadelphia, PA; and the Department of Orthopaedic Surgery, Faculty of Medicine Siriraj Hospital, Mahidol University, Bangkok, Thailand.

Received for publication June 4, 2013; accepted in revised form January 21, 2014.

The Hand Rehabilitation Foundation (King of Prussia, PA) provided funds for this study. Some of the volar locking plates used in this study were provided by Skeletal Dynamics and Acumed.

No benefits in any form have been received or will be received related directly or indirectly to the subject of this article.

Corresponding author: Roongsak Limthongthang, MD, Department of Orthopaedic Surgery, Faculty of Medicine Siriraj Hospital, Mahidol University, 2 Prannok Road, Bangkoknoi, Bangkok, Thailand 10700; e-mail: roongsak.lit@mahidol.ac.th.

0363-5023/■ ■-0001$36.00/0
http://dx.doi.org/10.1016/j.jhsa.2014.01.038

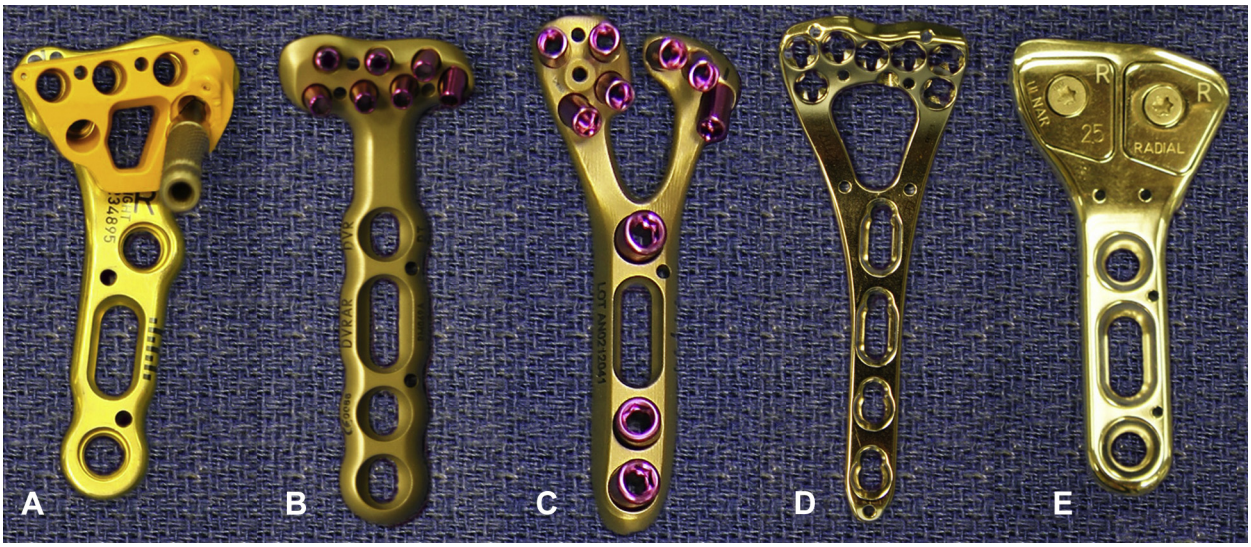

FIGURE 1: **A** Acu-Loc 2 Proximal VDR plate (Acumed, Hillsboro, OR), standard size, head width 24.4 mm, titanium alloy. **B** DVR Anatomic (Hand Innovations, Warsaw, IN), standard size, head width 24.4 mm, titanium alloy. **C** Geminus distal radius volar plate (Skeletal dynamics, Miami, FL), standard size, head width 24.5 mm, titanium alloy. **D** A 2.4-mm variable-angle LCP 2-column volar distal radius plate (Synthes, West Chester, PA), standard size 7-hole, head width 25.5 mm, stainless steel. **E** CoverLoc volar plate (Tornier, Bloomington, MN), head width 25 mm, stainless steel.

decade.[2] However, despite its popularity, VLP fixation predisposes patients to specific risks and complications, such as intra-articular screw placement, prominent hardware, and possible extensor and flexor tendon injury.[3] Before the introduction of VLPs, flexor tendon ruptures after distal radius fracture fixation were less frequent and most often reported to result from malunion, chronic use of steroids, prominent hardware, or the improper use of plates and screws.[4–8]

The flexor pollicis longus (FPL) and flexor digitorum profundus tendons travel close to the volar ridge of bone in the distal radial metaphysis, which is known as the watershed line.[9] This landmark is clinically important because placement of the VLP distal to the watershed line may be associated with increased rates of flexor tendon irritation, fraying, and ultimately, rupture. Furthermore, the final common pathway of flexor tendon rupture after VLP fixation appears to involve prominent implants at the watershed line.[10] Drobetz and Kutscha-Lissberg[11] reported FPL tendon ruptures in 12% of their population during the use of an early VLP design (Mathys, Salzburg, Austria). They concluded that plate design and distal plate placement contributed to tendon-related problems.

In an attempt to reduce the incidence of flexor tendon attritional injury and provide maximal stability, recent plate designs have enhanced anatomical contours, lower profiles, and variable-angle locking screws. Despite these design modifications, attritional flexor tendon injury continues to be problematic.[12,13]

The aims of this morphometric study were to evaluate volar plate prominence of various VLP designs and to assess the relationship of the FPL to the watershed line, because these parameters may be associated with flexor tendon attritional injury. Particular emphasis was placed on the FPL tendon, because this is one of the most frequently damaged structures after volar plate fixation. This information may aid surgeons in making a more informed decision during plate selection and placement.

MATERIALS AND METHODS

Twelve fresh-frozen, matched-pair, elbow-to-hand specimens were obtained for this study. Wrist x-rays were performed on all specimens, and 1 pair was excluded after a healed distal radius fracture was identified. The remaining 10 specimens were studied in detail. We studied 5 current designs of widely used plates. To be included, each plate was required to have an anatomical precontoured design, manufacturer-recommended fixation proximal to the watershed line, and a standard head size with a range between 24 and 26 mm. Figure 1 shows the details of each design. Throughout the text, the various VLP designs are denoted as plates A, B, C, D, and E.

Dissection, plate fixation, and data acquisition

Before dissection, we thawed the specimens at room temperature. To standardize our dissection and subsequent mapping of the path of the FPL, each specimen was

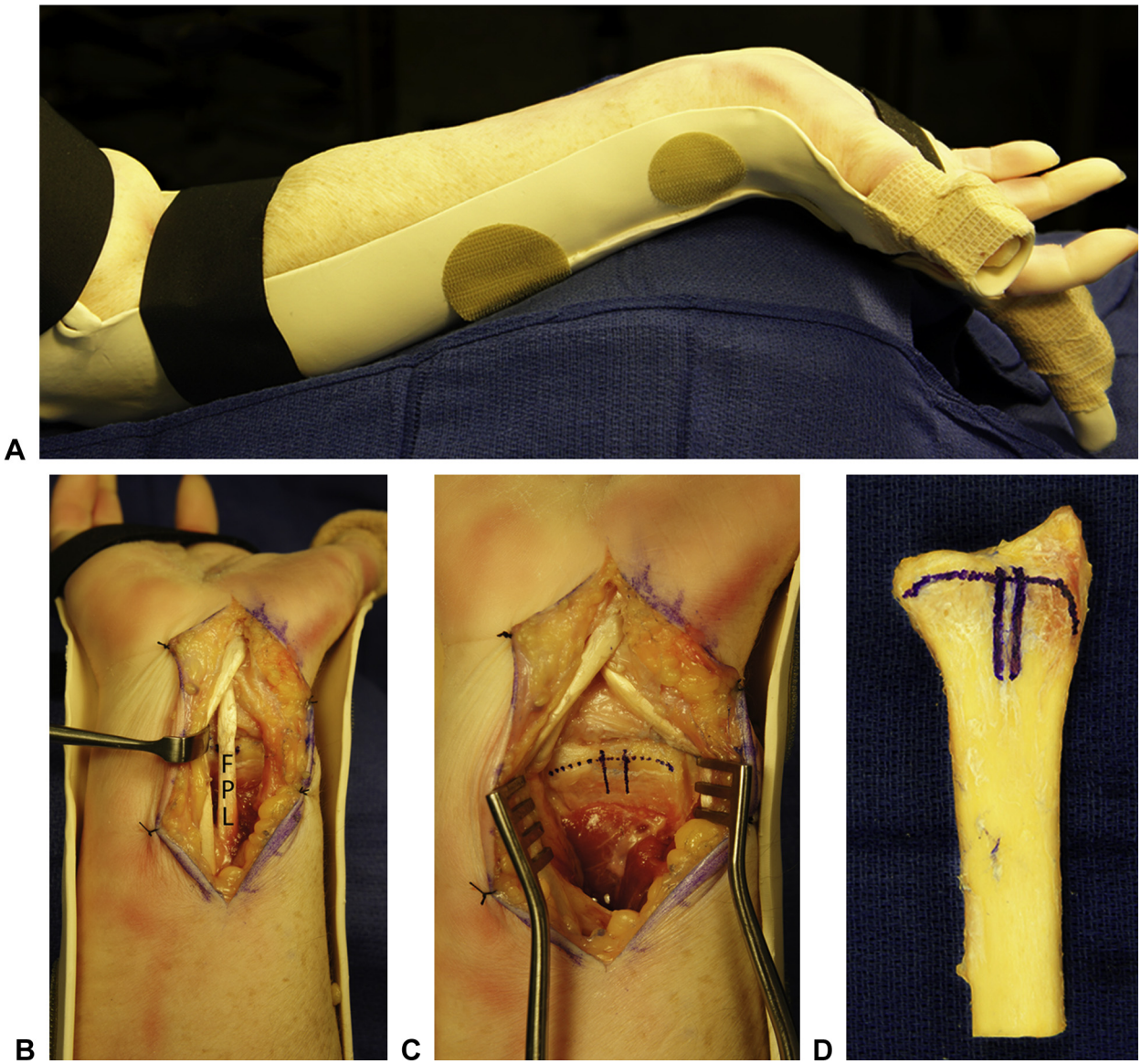

FIGURE 2: **A** Specimens were positioned in 60° wrist extension and 45° thumb abduction and full extension. **B** Position of the FPL in the cadaveric specimen. **C** The path of the FPL tendon and the watershed line were marked on the radius. **D** The distal radius was stripped of all soft tissue before 3-dimensional digitization.

stabilized in a custom-made long-arm orthosis that held the wrist in 60° extension, neutral deviation, and forearm supination. The middle finger was stabilized in full extension and the thumb was maintained in 45° abduction and full extension (Fig. 2). Wrist positioning was based on the study by Tanaka et al,[14] which demonstrated significantly increased pressure between the FPL and the volar plate's edge at 60° wrist extension.

Dissection was carried out through the interval between the flexor carpi radialis and the radial artery.[15,16] Throughout the dissection, the FPL was maintained in its predissection anatomical position by preserving the FPL muscle origin and carpal tunnel boundaries and maintaining the tension on the FPL tendon by stabilizing the wrist and thumb in the orthosis. The positions of the FPL over the distal radius and watershed line were then marked with a surgical marker (Fig. 2).

We then removed all soft tissues and transected the radius 15 cm proximal to its distal surface. The specimen was then fixed to a precalibrated automatic rotating and tilting platform of a 3-dimensional laser scanner system (Next Engine, Santa Monica, CA). The accuracy of this system was previously validated using a μCT scanner for small bone surfaces and achieved an average deviation of 53 μm,[17] which provided sufficient accuracy given our objectives. The specimen was scanned in its entirety from 14 angles in macro mode at a resolution of 1,550 data points/cm^2. The annotated

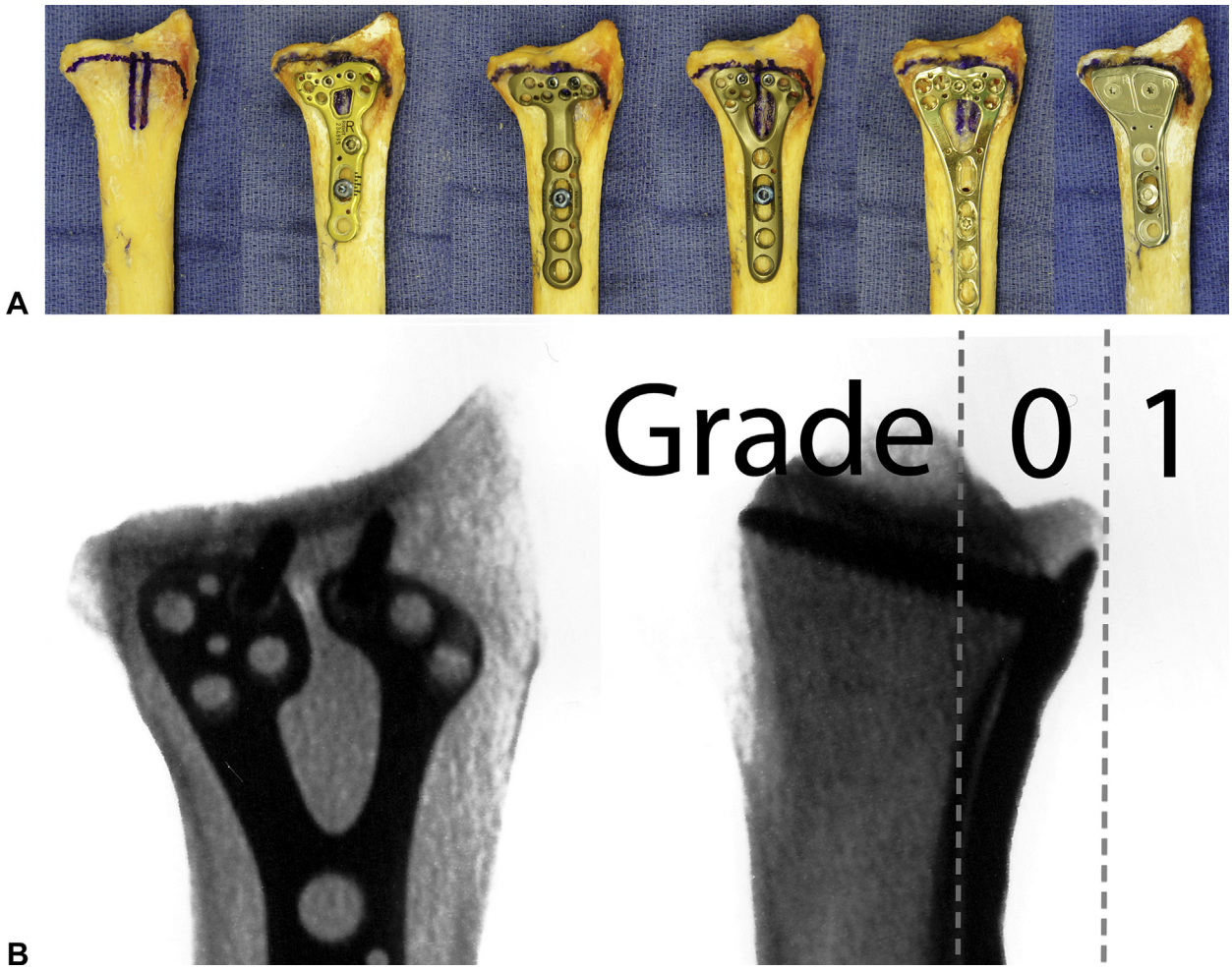

FIGURE 3: A Fixation of each plate on the same specimen. **B** Plate fixation was classified according to the radiographic system developed by Soong et al.[10]

distal radius was scanned and considered the reference model.

Each of the 5 plates was then fixed to each specimen by one surgeon. Therefore, there were 50 different plate–bone combinations. To reduce potential bias associated with the order of fixation, each plate design was fixed to the specimen in first, second, third, fourth, and fifth place, on 2 occasions. The aim of fixation was to position each plate in its proper anatomic fit, in similar axial alignment, and as close to the watershed line as possible to ensure distal screw placement close to the subchondral bone. No plates were bent to contour them to the specimens. The initial step involved plate fixation to the radial shaft with 1 nonlocking cortical screw that was drilled into the gliding slot hole. Fluoroscopy was used to adjust the plate and screw positions. We achieved optimization of the plate's position by sliding the plate distally to ensure that it was just proximal to the marked watershed line. After the optimal position was achieved, the proximal screw was tightened. Two compression screws for each system were then inserted through the distal row screw holes, aiming for screw placement within 2 mm of the subchondral bone, 1 on the radial side and 1 on the ulnar side. Plate fixation was classified according to the radiographic system developed by Soong et al,[10] in an attempt to objectively report the position of each plate (Fig. 3). Each plate–bone combination was then scanned using the same protocol as the reference bone model, and a test model was obtained. Most of the plates could be fixed to the radial shaft using the same screw hole, but when the initial gliding screw hole did not allow sufficient plate adjustment or became loose, another screw hole was drilled in the same axial direction.

The test models were automatically aligned with the reference model by using the best-fit alignment function (Geomagic Qualify 2012 software, Research Triangle Park, NC). Global registration of the models was then performed to fine-tune model alignment.

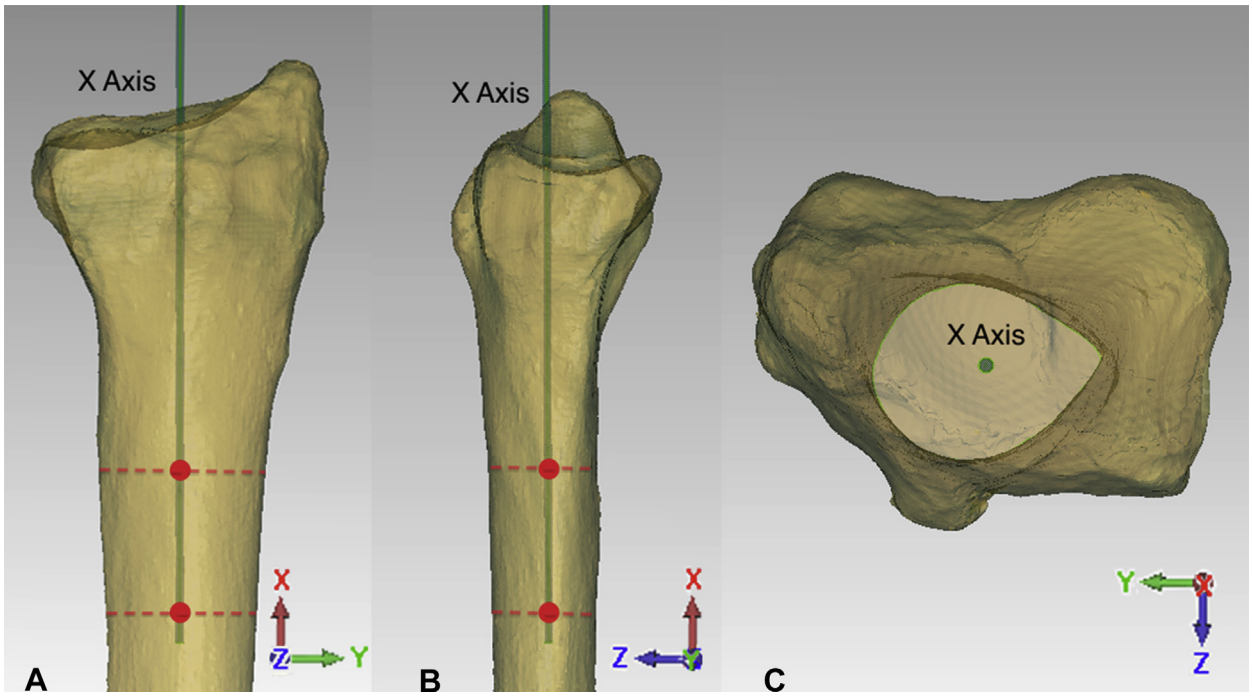

FIGURE 4: The reference coordinate system enabled standardized measurements for all models. The x axis was defined by 2 centroids (red points) along the axis of the radius 4 and 6 cm proximal to the joint surface and is demonstrated in the **A** anteroposterior and **B** lateral views. **C** The measurements of the prominent profile of each plate were based on the axial view.

Model processing and measurements

Coordinate system: The reference coordinate system was set to standardize the viewing axis and allow objective, reproducible measurements for all test models. The direction of the x axis was defined by 2 centroids along the longitudinal axis of the radial shaft 4 and 6 cm proximal to the joint surface (Fig. 4). The line passing the centroids of the lunate fossa and the radial styloid defined the direction of the y axis. The x−y plane was created based on the x and y axes. The z axis was automatically generated as the axis perpendicular to the x−y plane.

Parameters measured from 3-dimensional models: For the location of the FPL at the watershed line of the distal radius, the distance from the volar-ulnar corner of the distal radius to the midpoint between the 2 boundaries of the FPL at the level of the watershed line was measured to determine the location of the FPL. This distance was measured parallel to the y axis. The maximum width of the distal radius was also measured parallel to the y axis and was used to scale the distance from the volar-ulnar corner to the FPL tendon (expressed as a percentage of the maximum width) (Fig. 5).

Three additional quantitative measurements enabled us to evaluate plate prominence, which we considered to be 1 of many potential risk factors of flexor tendon injury. These measurements were as follows.

We measured total area of the prominent volar plate profile (A^T) to assess the plate prominence that may interfere with all of the overlying tendons that glide over the volar plate. Using the standardized y−z viewing plane (similar to an axial cut at the wrist) (Fig. 6), the area of the plate volarly prominent was manually selected, and the software calculated the surface area. This was repeated for all 5 plates for each specimen (Fig. 6).

We measured the area of the prominent volar plate profile directly beneath the path of the FPL (A^F) to assess plate prominence that could interfere with the FPL tendon as it glides over the volar plate. Using the standardized y−z viewing plane, the area of the plate prominence along the path of the FPL was manually selected, and the software calculated the surface area. This was repeated for all 5 plates for each specimen (Fig. 7).

We also measured the thickness of the prominent volar plate profile directly beneath the path of the FPL (T^F) to quantitatively assess plate prominence that could interfere with the FPL tendon as it glides over the edge of the plate. The thickness of the plate prominent to the watershed line was measured in a sagittal plane that was centered midway between the 2 lines that marked the boundaries of the FPL tendon (Fig. 8). When the edge of the plate was below the watershed line and could not be detected, this parameter was recorded as 0 mm.

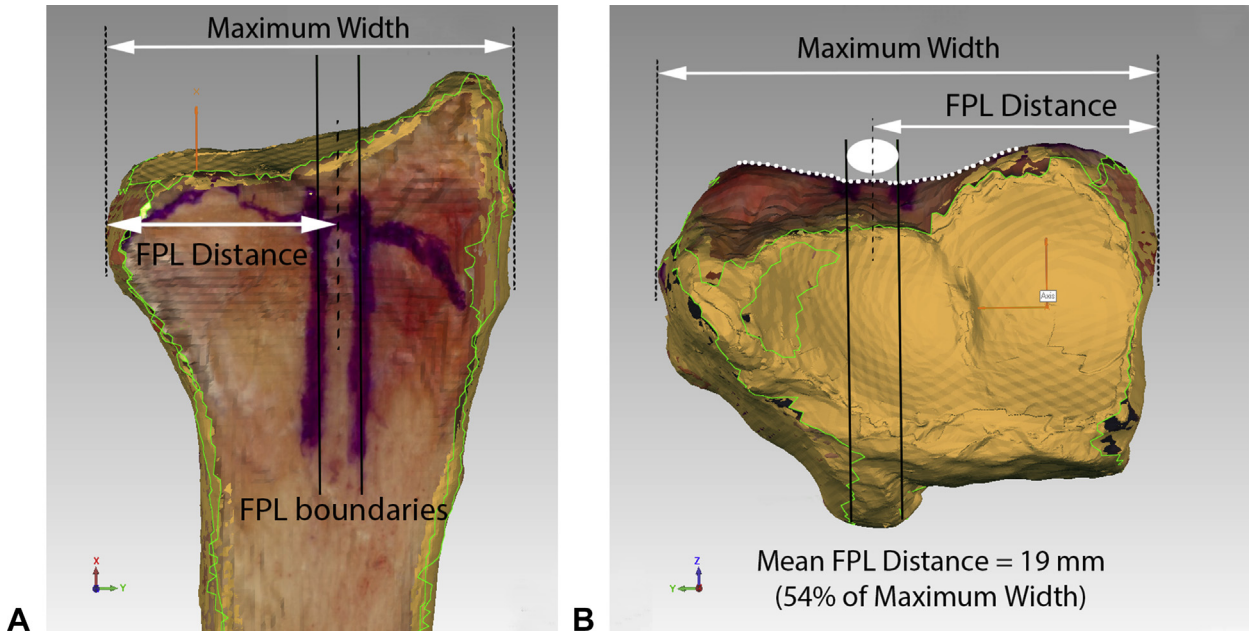

FIGURE 5: **A** Three-dimensional model with the FPL tendon path marked. The boundaries of the FPL were created directly over the marked lines. The position of the FPL at the distal radius was measured from the volar-ulnar corner of the distal radius to the center of the boundaries at the level of the watershed line. **B** The axial view shows the position of the FPL (ellipse) located in the trough of the watershed line (dotted line).

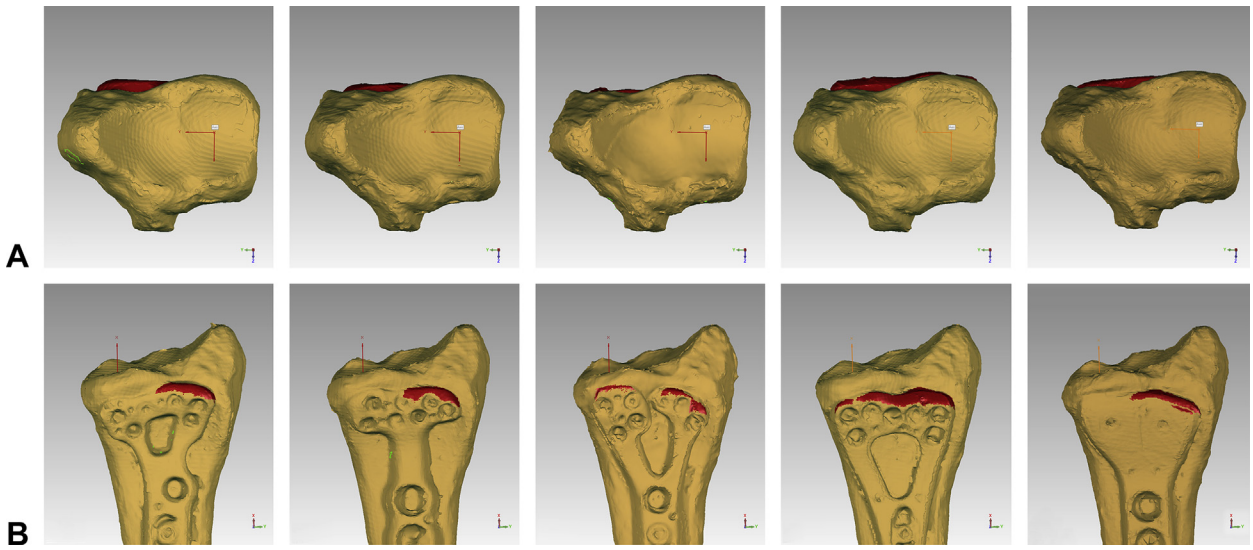

FIGURE 6: The prominent area of each plate's profile is highlighted in red (A^T). **A** Axial view (y−z viewing plane) for each plate design illustrating the prominent area of plate above the watershed line. **B** Volar view of each design showing the area of plate prominence (x−y viewing plane).

We did not measure the distance between the dorsal surface of the FPL and the volar edge of the plate because we observed the FPL to be in direct contact with the watershed line, especially during wrist extension. Therefore, at least *in vitro*, the distance between the dorsal aspect of the FPL and the plate's surface was close to 0 in every instance.

Statistical analysis

The Kolmogorov−Smirnov test indicated that the total area of plate prominence followed a normal distribution. Subsequently, 1-way analysis of variance was used to analyze numerical data. Bonferroni post hoc analysis was used when indicated. A 2-tailed *P* value less than .05 was considered statistically significant.

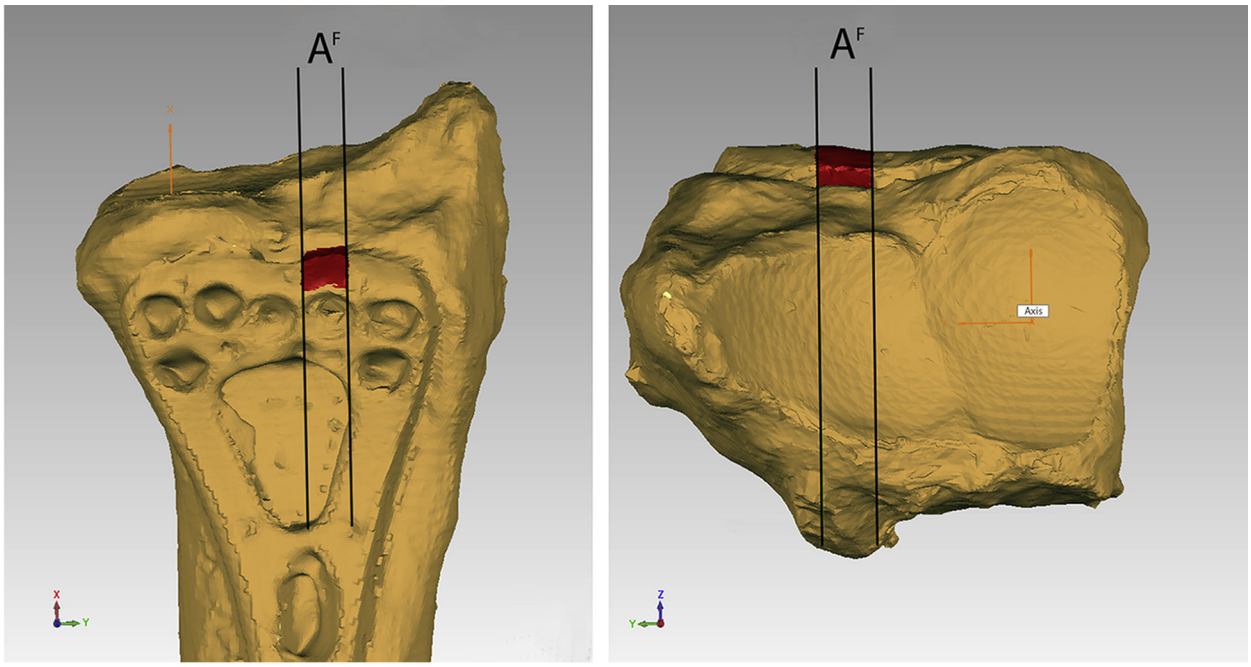

FIGURE 7: The prominent area of the volar plate directly beneath the path of the FPL is highlighted in red (A^F).

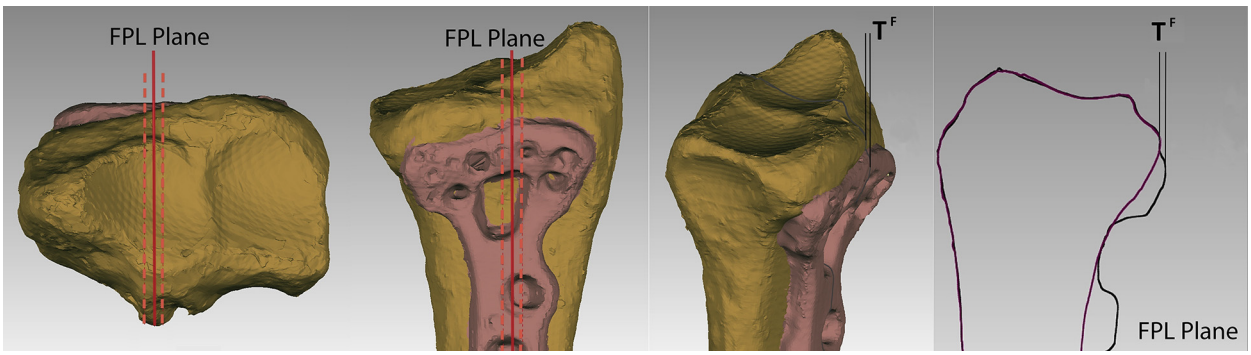

FIGURE 8: A 2-dimensional section created at the FPL plane centered between the FPL tendon boundaries (dotted lines). The thickness of the prominent profile of the volar plate directly beneath the path of the FPL is T^F.

RESULTS

There were 3 male and 2 female cadavers with a median age at death of 65 years (range, 36–76 y). The median body weight was 81 kg (range, 63–104 kg) and the median height was 178 cm (range, 157–182 cm). Table 1 lists the classifications and measurements.

Flexor pollicis longus location at distal radius

The average position of the FPL tendon from the volar-ulnar corner of the distal radius was 19 mm (range, 16–21 mm) or 54% (range, 47% to 62%) of the maximum width of the distal radius.

Evaluation of plate position

Lateral view fluoroscopic examination revealed that 90% of all specimens were classified as Soong grade 0; that is, these plates were not prominent to the volar rim of the distal radius. The other 10% were classified as grade 1.

Plate profile and prominence

The mean total surface area of plate prominence (A^T) (Fig. 6) was 36 mm^2 for all designs. Plate C had the lowest profile, which was significantly less than plate D and plate E, but not significantly different from plate A or plate B (Table 1).

The mean area of the prominent volar plate directly beneath the path of the FPL (A^F) (Fig. 7) was 10 mm^2 for all designs. Plate C had the lowest area, which was significantly less than all other plates.

The mean thickness of the prominent profile directly beneath the path of the FPL tendon (T^F) (Fig. 8) for all designs was 0.7 ± 0.7 mm. Plate C was the thinnest, and was significantly thinner than

TABLE 1. Summary of Results

Plate Design	Evaluation of Plate Position: Classification of Soong et al[10] Grade 0	Evaluation of Plate Position: Classification of Soong et al[10] Grade 1	Prominent Profile of Plate: A^T, mm^2	Prominent Profile of Plate: A^F, mm^2	Prominent Profile of Plate: T^F, mm
A	9	1	33 ± 7	9 ± 3	0.6 ± 0.5
B	10	0	31 ± 16	9 ± 5	0.6 ± 0.6
C	9	1	18 ± 11*	2 ± 2†	0.1 ± 0.2‡
D	8	2	56 ± 23*	15 ± 5	1.2 ± 0.9‡
E	9	1	42 ± 12*	14 ± 5	1.2 ± 0.8
Total	45	5	36 ± 19	10 ± 6	0.7 ± 0.7

A^T, total area of prominent volar plate profile; A^F, area of prominent volar plate profile directly beneath the path of the FPL; T^F, thickness of prominent volar plate profile directly beneath the path of the FPL.
*Plate C versus D ($P < .001$), plate C versus E ($P = .007$).
†Plate C versus all other plates ($P \leq .001$).
‡Plate C versus D ($P = .040$).

plate D. There were no statistically significant differences between the other designs.

DISCUSSION

Flexor tendon injury is a widely recognized complication of VLP fixation.[3] Despite modern low-profile anatomical designs, flexor tendon injury remains a problem, with an incidence of up to 2% in recent studies.[10,13,18] The cause of flexor tendon injury has been attributed to fracture malunion and hardware prominence owing to incomplete reduction or poor plate placement.[10,13,18]

We found that the FPL at the watershed line was located at an average of 19 mm lateral to the volar-ulnar corner of the radius, approximately at the midpoint of the maximum width of the distal radius. In the axial view, this location was not the most volarly prominent segment of the watershed line, which was in fact located on the ulnar side.[19] Rather, the gliding path of the FPL tendon was located in the trough of the watershed line, within a sulcus between the scaphoid and lunate fossas. Orbay referred to this area as the interfossa sulcus (Orbay JL, presented at the American Association for Hand Surgery annual meeting, 2013) (Fig. 5).

Soong et al[10] developed a classification scheme for the evaluation of VLP placement. In their series of 168 distal radius fractures, plates that did not surpass a line tangent to the volar rim of the distal radius on lateral x-rays were classified as grade 0. In that group, the authors found no FPL ruptures. Plates that were positioned volar to this line but proximal to the volar lip were classified as grade 1 and were associated with a flexor tendon rupture rate of almost 2%. When the plates were distal to the volar rim of the distal radius (grade 2), the rupture rate exceeded 4%. White et al[18] reported 5 FPL ruptures in 999 patients. However, they were not able to find a significant correlation between the Soong classification and FPL ruptures. In our study, 90% of specimens were classified as grade 0 and the other 10% as grade 1. Furthermore, T^F beneath the path of FPL tendon ranged between 0.6 and 1.2 mm. Therefore, despite a grade 0 position on lateral x-ray, the potential remained for the development of gliding friction between the plate and the FPL. Tanaka et al[14] studied contact pressures between the FPL and the VLP in various plate positions. They found that despite proper placement of volar plates, significant increases in pressure beneath the FPL tendon arose compared with nonplated specimens in 60° wrist extension. The contact pressure was even higher when the position of the plate was moved 2.5 mm distally.

The manufacturers of all plates used in this study recommend fixation proximal to the watershed line. Although VLPs are designed to accommodate the morphology of the distal radius, including the shape of the watershed line and the lunate facet buttress, each design has its nuances. For example, some plates have a longer extension along the medial rim to support the lunate facet. Others possess a longer extension along the lateral rim, which may produce a higher potential of flexor tendons irritation.[10] Given the location of the FPL at approximately the midpoint of the distal radius, a number of manufacturers have designed their plates to have a central concave profile. In theory, this should decrease FPL tendon irritation.

In this study, titanium alloy plates had lower profiles than stainless-steel plates. Titanium wear particles

have been postulated to cause tenosynovitis, which may predispose tendons to rupture.[20] However, later studies found that regardless of the plate's material, placement of the plate directly beneath the gliding tendons may cause tendon strain, leading to a fibrotic reaction, degeneration, and eventual rupture.[21,22] In the plates fabricated from titanium, no significant differences were identified when the total area and thickness of the prominent profiles were compared. However, when the FPL gliding area was compared, plate C had a significantly smaller area relative to the other 2 titanium plates (A and B). This finding is a result of the Y-shaped design, where the bridging segment of the plate between the radial and intermediate columns has been removed.

A lower profile of 1 design over another may not necessarily decrease the risk for tendon rupture.[23] Clinical familiarity with the plate system may influence the complication rate more so than plate design.[3] Soong et al[10] found that plates that were not commonly used were positive predictors of plate-related complications.

The limitations of the study include a small sample size of cadavers as well as plates. Second, 5 plates were fixed to the same specimen, which may have affected screw placement and fixation. However, we balanced the order of plate placement to minimize this limitation. Third, we studied only 5 designs, and many designs are currently in circulation. However, the findings of the relationships among the various VLP designs, the FPL, and the watershed line might be extrapolated to morphologically similar designs. At the least, we have shown that there are nuances to each system, of which the operating surgeon should be aware.

The strength of this study was the use of precise 3-dimensional digitization to measure a small, complex surface area, which is difficult to measure with conventional measurement techniques. Using the inspection software, we were able to standardize our reference axes and measurements in an attempt to maintain consistency and objectivity and limit human error.

These data may help guide implant design considerations and assist the surgeon in better understanding implant morphology as it relates to the possibility of flexor tendon injury. Future directions may include analyzing other commercially available VLPs and their specific design profiles, with the ultimate goal of optimizing construct placement and minimizing plate-related complications.

REFERENCES

1. Orbay JL. The treatment of unstable distal radius fractures with volar fixation. *Hand Surg*. 2000;5(2):103–112.
2. Fanuele J, Koval KJ, Lurie J, Zhou W, Tosteson A, Ring D. Distal radial fracture treatment: what you get may depend on your age and address. *J Bone Joint Surg Am*. 2009;91(6):1313–1319.
3. Soong M, van Leerdam R, Guitton TG, Got C, Katarincic J, Ring D. Fracture of the distal radius: risk factors for complications after locked volar plate fixation. *J Hand Surg Am*. 2011;36(1):3–9.
4. Takami H, Takahashi S, Ando M. Attritional flexor tendon ruptures after a malunited intra-articular fracture of the distal radius. *Arch Orthop Trauma Surg*. 1997;116(8):507–509.
5. Wada A, Ihara F, Senba H, Nomura S. Attritional flexor tendon ruptures due to distal radius fracture and associated with volar displacement of the distal ulna: a case report. *J Hand Surg Am*. 1999;24(3):534–537.
6. Fuller DJ. The Ellis plate operation for Smith's fracture. *J Bone Joint Surg Br*. 1973;55(1):173–178.
7. Bell JS, Wollstein R, Citron ND. Rupture of flexor pollicis longus tendon: a complication of volar plating of the distal radius. *J Bone Joint Surg Br*. 1998;80(2):225–226.
8. Nunley JA, Rowan PR. Delayed rupture of the flexor pollicis longus tendon after inappropriate placement of the pi plate on the volar surface of the distal radius. *J Hand Surg Am*. 1999;24(6):1279–1280.
9. Orbay JL, Touhami A. Current concepts in volar fixed-angle fixation of unstable distal radius fractures. *Clin Orthop Relat Res*. 2006;(445):58–67.
10. Soong M, Earp BE, Bishop G, Leung A, Blazar P. Volar locking plate implant prominence and flexor tendon rupture. *J Bone Joint Surg Am*. 2011;93(4):328–335.
11. Drobetz H, Kutscha-Lissberg E. Osteosynthesis of distal radial fractures with a volar locking screw plate system. *Int Orthop*. 2003;27(1):1–6.
12. Cross AW, Schmidt CC. Flexor tendon injuries following locked volar plating of distal radius fractures. *J Hand Surg Am*. 2008;33(2):164–167.
13. Casaletto JA, Machin D, Leung R, Brown DJ. Flexor pollicis longus tendon ruptures after palmar plate fixation of fractures of the distal radius. *J Hand Surg Eur Vol*. 2009;34(4):471–474.
14. Tanaka Y, Aoki M, Izumi T, Fujimiya M, Yamashita T, Imai T. Effect of distal radius volar plate position on contact pressure between the flexor pollicis longus tendon and the distal plate edge. *J Hand Surg Am*. 2011;36(11):1790–1797.
15. Orbay JL, Badia A, Indriago IR, et al. The extended flexor carpi radialis approach: a new perspective for the distal radius fracture. *Tech Hand Up Extrem Surg*. 2001;5(4):204–211.
16. Henry AK. *Extensile Exposure*. 2nd ed. Baltimore: Williams and Wilkins; 1957:67.
17. Slizewski A, Friess M, Semal P. Surface scanning of anthropological specimens: nominal-actual comparison with low cost laser scanner and high end fringe light projection surface scanning systems. *Quartär*. 2010;57:179–187.
18. White BD, Nydick JA, Karsky D, Williams BD, Hess AV, Stone JD. Incidence and clinical outcomes of tendon rupture following distal radius fracture. *J Hand Surg Am*. 2012;37(10):2035–2040.
19. Imatani J, Akita K, Yamaguchi K, Shimizu H, Kondou H, Ozaki T. An anatomical study of the watershed line on the volar, distal aspect of the radius: implications for plate placement and avoidance of tendon ruptures. *J Hand Surg Am*. 2012;37(8):1550–1554.
20. Sinicropi SM, Su BW, Raia FJ, Parisien M, Strauch RJ, Rosenwasser MP. The effects of implant composition on extensor tenosynovitis in a canine distal radius fracture model. *J Hand Surg Am*. 2005;30(2):300–307.
21. Nazzal A, Lozano-Calderon S, Jupiter JB, Rosenzweig JS, Randolph MA, Lee SG. A histologic analysis of the effects of stainless steel and titanium implants adjacent to tendons: an experimental rabbit study. *J Hand Surg Am*. 2006;31(7):1123–1130.
22. Cohen MS, Turner TM, Urban RM. Effects of implant material and plate design on tendon function and morphology. *Clin Orthop Relat Res*. 2006;(445):81–90.
23. Buzzell JE, Weikert DR, Watson JT, Lee DH. Precontoured fixed-angle volar distal radius plates: a comparison of anatomic fit. *J Hand Surg Am*. 2008;33(7):1144–1152.